FERMILAB-PUB-21-276-ND

Extended search for supernova-like neutrinos in NOvA coincident with LIGO/Virgo detections

M. A. Acero,[2] P. Adamson,[12] L. Aliaga,[12] N. Anfimov,[26] A. Antoshkin,[26] E. Arrieta-Diaz,[28] L. Asquith,[41] A. Aurisano,[6] A. Back,[24] C. Backhouse,[46] M. Baird,[20,41,47] N. Balashov,[26] P. Baldi,[25] B. A. Bambah,[17] S. Bashar,[45] K. Bays,[4,19] R. Bernstein,[12] V. Bhatnagar,[34] B. Bhuyan,[14] J. Bian,[25,31] J. Blair,[16] A. C. Booth,[41] R. Bowles,[20] C. Bromberg,[29] N. Buchanan,[8] A. Butkevich,[22] S. Calvez,[8] T. J. Carroll,[44,50] E. Catano-Mur,[49] B. C. Choudhary,[10] A. Christensen,[8] T. E. Coan,[39] M. Colo,[49] L. Corwin,[51] L. Cremonesi,[36,46] G. S. Davies,[32,20] P. F. Derwent,[12] P. Ding,[12] Z. Djurcic,[1] M. Dolce,[45] D. Doyle,[8] D. Dueñas Tonguino,[6] E. C. Dukes,[47] H. Duyang,[38] S. Edayath,[7] R. Ehrlich,[47] M. Elkins,[24] E. Ewart,[20] G. J. Feldman,[15] P. Filip,[23] J. Franc,[9] M. J. Frank,[37] H. R. Gallagher,[45] R. Gandrajula,[29,47] F. Gao,[35] A. Giri,[18] R. A. Gomes,[13] M. C. Goodman,[1] V. Grichine,[27] M. Groh,[8,20] R. Group,[47] B. Guo,[38] A. Habig,[30] F. Hakl,[21] A. Hall,[47] J. Hartnell,[41] R. Hatcher,[12] A. Hatzikoutelis,[43,*] H. Hausner,[50] K. Heller,[31] J. Hewes,[6] A. Himmel,[12] A. Holin,[46] J. Huang,[44] B. Jargowsky,[25] J. Jarosz,[8] F. Jediny,[9] C. Johnson,[8] M. Judah,[8,35] I. Kakorin,[26] D. Kalra,[34] D. M. Kaplan,[19] A. Kalitkina,[26] R. Keloth,[7] O. Klimov,[26] L. W. Koerner,[16] L. Kolupaeva,[26] S. Kotelnikov,[27] R. Kralik,[41] Ch. Kullenberg,[26] M. Kubu,[9] A. Kumar,[34] C. D. Kuruppu,[38] V. Kus,[9] T. Lackey,[20] K. Lang,[44] P. Lasorak,[41] J. Lesmeister,[16] S. Lin,[8] A. Lister,[50] J. Liu,[25] M. Lokajicek,[23] S. Magill,[1] M. Manrique Plata,[20] W. A. Mann,[45] M. L. Marshak,[31] M. Martinez-Casales,[24] V. Matveev,[22] B. Mayes,[41] D. P. Méndez,[41] M. D. Messier,[20] H. Meyer,[48] T. Miao,[12] W. H. Miller,[31] S. R. Mishra,[38] A. Mislivec,[31] R. Mohanta,[17] A. Moren,[30] A. Morozova,[26] W. Mu,[12] L. Mualem,[4] M. Muether,[48] S. Mufson,[20] K. Mulder,[46] D. Naples,[35] N. Nayak,[25] J. K. Nelson,[49] R. Nichol,[46] E. Niner,[12] A. Norman,[12] A. Norrick,[12] T. Nosek,[5] H. Oh,[6] A. Olshevskiy,[26] T. Olson,[45] J. Ott,[25] J. Paley,[12] R. B. Patterson,[4] G. Pawloski,[31] O. Petrova,[26] R. Petti,[38] D. D. Phan,[44,46] R. K. Plunkett,[12] J. C. C. Porter,[41] A. Rafique,[1] F. Psihas,[20,44] V. Raj,[4] M. Rajaoalisoa,[6] B. Ramson,[12] B. Rebel,[12,50] P. Rojas,[8] V. Ryabov,[27] O. Samoylov,[26] M. C. Sanchez,[24] S. Sánchez Falero,[24] P. Shanahan,[12] A. Sheshukov,[26] P. Singh,[10] V. Singh,[3] E. Smith,[20] J. Smolik,[9] P. Snopok,[19] N. Solomey,[48] A. Sousa,[6] K. Soustruznik,[5] M. Strait,[31] L. Suter,[12] A. Sutton,[47] S. Swain,[33] C. Sweeney,[46] B. Tapia Oregui,[44] P. Tas,[5] T. Thakore,[6] R. B. Thayyullathil,[7] J. Thomas,[46,50] E. Tiras,[11,24] J. Tripathi,[34] J. Trokan-Tenorio,[49] A. Tsaris,[12] Y. Torun,[19] J. Urheim,[20] P. Vahle,[49] Z. Vallari,[4] J. Vasel,[20] P. Vokac,[9] T. Vrba,[9] M. Wallbank,[6] T. K. Warburton,[24] M. Wetstein,[24] D. Whittington,[42,20] D. A. Wickremasinghe,[12] S. G. Wojcicki,[40] J. Wolcott,[45] W. Wu,[25] Y. Xiao,[25] A. Yallappa Dombara,[42] K. Yonehara,[12] S. Yu,[1,19] Y. Yu,[19] S. Zadorozhnyy,[22] J. Zalesak,[23] Y. Zhang,[41] and R. Zwaska[12]

(The NOvA Collaboration)

[1] *Argonne National Laboratory, Argonne, Illinois 60439, USA*
[2] *Universidad del Atlantico, Carrera 30 No. 8-49, Puerto Colombia, Atlantico, Colombia*
[3] *Department of Physics, Institute of Science, Banaras Hindu University, Varanasi, 221 005, India*
[4] *California Institute of Technology, Pasadena, California 91125, USA*
[5] *Charles University, Faculty of Mathematics and Physics, Institute of Particle and Nuclear Physics, Prague, Czech Republic*
[6] *Department of Physics, University of Cincinnati, Cincinnati, Ohio 45221, USA*
[7] *Department of Physics, Cochin University of Science and Technology, Kochi 682 022, India*
[8] *Department of Physics, Colorado State University, Fort Collins, CO 80523-1875, USA*
[9] *Czech Technical University in Prague, Brehova 7, 115 19 Prague 1, Czech Republic*
[10] *Department of Physics and Astrophysics, University of Delhi, Delhi 110007, India*
[11] *Department of Physics, Erciyes University, Kayseri 38030, Turkey*
[12] *Fermi National Accelerator Laboratory, Batavia, Illinois 60510, USA*
[13] *Instituto de Física, Universidade Federal de Goiás, Goiânia, Goiás, 74690-900, Brazil*
[14] *Department of Physics, IIT Guwahati, Guwahati, 781 039, India*
[15] *Department of Physics, Harvard University, Cambridge, Massachusetts 02138, USA*
[16] *Department of Physics, University of Houston, Houston, Texas 77204, USA*
[17] *School of Physics, University of Hyderabad, Hyderabad, 500 046, India*
[18] *Department of Physics, IIT Hyderabad, Hyderabad, 502 205, India*
[19] *Illinois Institute of Technology, Chicago IL 60616, USA*
[20] *Indiana University, Bloomington, Indiana 47405, USA*
[21] *Institute of Computer Science, The Czech Academy of Sciences, 182 07 Prague, Czech Republic*
[22] *Institute for Nuclear Research of Russia, Academy of Sciences 7a, 60th October Anniversary prospect, Moscow 117312, Russia*
[23] *Institute of Physics, The Czech Academy of Sciences, 182 21 Prague, Czech Republic*
[24] *Department of Physics and Astronomy, Iowa State University, Ames, Iowa 50011, USA*
[25] *Department of Physics and Astronomy, University of California at Irvine, Irvine, California 92697, USA*
[26] *Joint Institute for Nuclear Research, Dubna, Moscow region 141980, Russia*

This document was prepared by NOvA Collaboration using the resources of the Fermi National Accelerator Laboratory (Fermilab), a U.S. Department of Energy, Office of Science, HEP User Facility. Fermilab is managed by Fermi Research Alliance, LLC (FRA), acting under Contract No. DE-AC02-07CH11359.

[27] Nuclear Physics and Astrophysics Division, Lebedev Physical Institute, Leninsky Prospect 53, 119991 Moscow, Russia
[28] Universidad del Magdalena, Carrera 32 No 22-08 Santa Marta, Colombia
[29] Department of Physics and Astronomy, Michigan State University, East Lansing, Michigan 48824, USA
[30] Department of Physics and Astronomy, University of Minnesota Duluth, Duluth, Minnesota 55812, USA
[31] School of Physics and Astronomy, University of Minnesota Twin Cities, Minneapolis, Minnesota 55455, USA
[32] University of Mississippi, University, Mississippi 38677, USA
[33] National Institute of Science Education and Research, Khurda, 752050, Odisha, India
[34] Department of Physics, Panjab University, Chandigarh, 160 014, India
[35] Department of Physics, University of Pittsburgh, Pittsburgh, Pennsylvania 15260, USA
[36] School of Physics and Astronomy, Queen Mary University of London, London E1 4NS, United Kingdom
[37] Department of Physics, University of South Alabama, Mobile, Alabama 36688, USA
[38] Department of Physics and Astronomy, University of South Carolina, Columbia, South Carolina 29208, USA
[39] Department of Physics, Southern Methodist University, Dallas, Texas 75275, USA
[40] Department of Physics, Stanford University, Stanford, California 94305, USA
[41] Department of Physics and Astronomy, University of Sussex, Falmer, Brighton BN1 9QH, United Kingdom
[42] Department of Physics, Syracuse University, Syracuse NY 13210, USA
[43] Department of Physics and Astronomy, University of Tennessee, Knoxville, Tennessee 37996, USA
[44] Department of Physics, University of Texas at Austin, Austin, Texas 78712, USA
[45] Department of Physics and Astronomy, Tufts University, Medford, Massachusetts 02155, USA
[46] Physics and Astronomy Department, University College London, Gower Street, London WC1E 6BT, United Kingdom
[47] Department of Physics, University of Virginia, Charlottesville, Virginia 22904, USA
[48] Department of Mathematics, Statistics, and Physics, Wichita State University, Wichita, Kansas 67206, USA
[49] Department of Physics, William & Mary, Williamsburg, Virginia 23187, USA
[50] Department of Physics, University of Wisconsin-Madison, Madison, Wisconsin 53706, USA
[51] South Dakota School of Mines and Technology, Rapid City, South Dakota 57701, USA

A search is performed for supernova-like neutrino interactions coincident with 76 gravitational wave events detected by the LIGO/Virgo Collaboration. For 40 of these events, full readout of the time around the gravitational wave is available from the NOvA Far Detector. For these events, we set limits on the fluence of the sum of all neutrino flavors of $F < 7(4) \times 10^{10}\,\mathrm{cm}^{-2}$ at 90% C.L. assuming energy and time distributions corresponding to the Garching supernova models with masses $9.6(27)\,\mathrm{M}_\odot$. Under the hypothesis that any given gravitational wave event was caused by a supernova, this corresponds to a distance of $r > 29(50)\,\mathrm{kpc}$ at 90% C.L. Weaker limits are set for other gravitational wave events with partial Far Detector data and/or Near Detector data.

I. INTRODUCTION

Multimessenger astronomy is a rapidly expanding field, with exciting opportunities to simultaneously observe violent astrophysical events using gravitational waves (GW), electromagnetic radiation, cosmic rays, and neutrinos. To date, a single gravitational wave event has been associated with electromagnetic activity [1–3], and none have been associated with the other channels. Not all gravitational waves and gravitational wave candidates to date have been identified by the LIGO/Virgo Collaboration (LVC) with a particular production mechanism [4]. Although all clearly identified events are associated with compact object mergers, there remains the possibility that one or more was caused by a supernova, which are expected to produce gravitational waves, but with great uncertainty in predictions of the signal strength [5]. These potential supernovae may have evaded optical detection either because they were obscured by dust in the central Galaxy, or because they were "failed" supernovae in which the star collapsed, but did not explode [6].

In a previous paper [7] we described a broad search for signals, across the MeV to TeV range, associated with 26 gravitational wave events. We now focus on the possibility of detecting supernova-like neutrinos and present an improved search using the now-available larger catalog of gravitational wave events. The paper is organized as follows. In Section II, we introduce the NOvA detectors. Section III details the data set used in this analysis. Section IV explains how we simulate supernova neutrino interactions. Section V describes the improved selection of supernova-like neutrinos. Finally, Section VI gives the results.

II. DETECTORS

The NOvA experiment consists of two similar detectors, the Near Detector (ND) and the Far Detector (FD). The ND is located at the Fermi National Accelerator Laboratory (Fermilab), 100 m underground, while the FD is located near Ash River, Minnesota, on the surface with a modest overburden consisting of 1.25 m of concrete covered with 16 cm of barite gravel.

The NOvA detectors are segmented liquid scintillator tracking calorimeters. Alternating planes of cells are oriented horizontally and vertically, forming two views that can be used to reconstruct three-dimensional positions.

* now at San José State University

The cells have a cross section of 4 cm by 6 cm and are 15.5 m (3.8 m) long in the FD (ND). The FD has 896 planes of cells and a total mass of 14 kt, whereas the ND has 214 planes and a total mass of 300 t. The last 20 planes at the north end of the ND are a muon catcher. They are interleaved with ten 10-cm-thick planes of steel for the purpose of measuring the energy of muons produced in beam interactions. The FD has no similar structure. The detectors are described in more detail elsewhere [8].

Light produced in the scintillator is collected by wavelength-shifting fibers and converted into electrical signals using avalanche photodiodes. These signals are continuously digitized at 2 MHz at the FD and 8 MHz at the ND. Samples rising above a threshold, called *hits*, are retained for further processing. Hits from all channels are collected into 50 μs blocks and can be saved for offline analysis if a software trigger requests them within about 20 minutes for the Far Detector and 30 minutes at the Near Detector. Triggers can either be based on the content of the data or on external signals. Two of the latter type of triggers are used in this analysis. First, when LVC publishes an observation of a gravitational wave candidate over the Gamma-ray Coordinates Network, we respond by reading out 45 s of continuous data from both the ND and FD, beginning 5.16 s prior to the gravitational wave timestamp. Second, we run a minimum bias pulser trigger on the FD which reads out 550 μs segments of data at a rate of 10 Hz. When only pulser data is available, we use a window of 1000 s centered on the gravitational wave timestamp to match the convention established by other neutrino observatories.

The NOvA detectors are exposed to Fermilab's NuMI beam [9], a wideband neutrino beam with a peak at 2 GeV consisting mainly of either ν_μ or $\bar{\nu}_\mu$, depending on the operating mode. Typically, the beam is operated October through June with pulses of 10 μs separated by 1.3 s. For the purposes of the analysis reported here, the beam has no impact on the FD data since the number of beam neutrino interactions is negligible. However, it is a source of background at the ND; a procedure to remove beam backgrounds is detailed in Section V.

III. DATA SET

Table I shows a summary of NOvA data collected for each of the gravitational wave events announced by LVC to date in their two catalogs [4, 10] and via the Gamma-ray Coordinates Network [11–40]. With the exception of four gravitational wave events, at least one of the NOvA detectors was operating and taking useful data for each event. LVC issued public triggers beginning with their "O3" run period in 2019; prior to that point, NOvA has only the FD pulser data. Thirteen events in O3 were only announced in the second LVC catalog and not via public trigger; we only have FD pulser data for these as well.

Of the remaining 52 GW events that did have public triggers, we recorded all or part of the desired 45 s of continuous data at the FD for 32 events, and at the ND for 40. In five cases, the ND recorded full readouts when the FD did not because it has a deeper data buffer. At each detector, data is read out approximately in time order; alerts that arrived when the data was near the end of the buffer resulted in partial readouts, as shown in the table. In the remaining three cases, the FD was down and the ND was up.

IV. SIMULATION

Supernova neutrino interactions are simulated for use in training the selector and for assessing signal significance. The simulation is based on the Garching 9.6 $M_\odot$ and 27 $M_\odot$ supernova flux models [41], with neutrino interactions produced with GENIE v3.0.6 [42], and the resulting particles tracked through the detector geometry using GEANT4 v10.4.2 [43]. The simulation only includes neutrinos above 10 MeV, with inverse beta decay on hydrogen (IBD) and electron elastic scattering (ES) interactions included. Since NOvA is hydrocarbon-based, IBD strongly dominates over ES. IBD is the most important interaction for NOvA because it has a large cross section and produces a high energy positron. The mean positron energy produced in the 9.6(27) $M_\odot$ simulation is 19.0(21.2) MeV.

In IBD interactions, both positrons and neutrons are simulated. Although NOvA is primarily sensitive to positrons and electrons, the 8 MeV of gammas from neutron capture on ^{35}Cl is also visible. The NOvA detectors are 16% chlorine by mass. After selection cuts, the FD has no significant sensitivity to electrons and positrons below 10 MeV, however, the ND is still marginally sensitive at this energy, so the simulation somewhat undercounts the neutrino interactions that would be selected in a real supernova.

Besides undercounting low energy neutrino interactions, the simulation also does not include various interaction channels on carbon such as $\nu_e + {}^{12}\mathrm{C} \to e^- + {}^{12}\mathrm{N}$, nor similar channels involving other isotopes in the NOvA materials, although in many cases, these interactions would be easily visible. The limits set below are therefore conservative, although IBD would dominate over these other channels even if they were included. We use a model without neutrino oscillations or other flavor-changing effects because there is not enough information available to know whether these effects would increase or decrease the number of neutrinos observed by NOvA [41].

V. ANALYSIS

Relative to our previous report [7], the clustering algorithm for grouping hits into supernova neutrino event candidates has been greatly improved. Previously, a cluster was defined as a pair of hits with one hit in each view.

TABLE I. Summary of NOvA data taking during GW events [4, 10–40] and fluence limits. The limits on the two supernova models, given in the rightmost two columns, are at 90% C.L. and are in units of $10^{10}\,\mathrm{cm}^{-2}$. When continuous data was read out in response to an LVC trigger, the number of seconds read is given for each detector. Otherwise ("untriggered"), pulser data is used in the case of the FD, and the ND is not used. In some cases one or both detectors were not running ("no data") and in two cases the FD was running, but not taking good data ("bad"). Events above the line on the left have been considered by NOvA before; above and below the line events are arranged chronologically.

Name	ND	FD	$SN_{27\odot}$	$SN_{9.6\odot}$
GW150914	Untriggered	Bad	—	—
GW151012	Untriggered	No data	—	—
GW151226	Untriggered	Untriggered	110	190
GW170104	Untriggered	Untriggered	300	500
GW170608	Untriggered	Untriggered	400	700
GW170729	Untriggered	Untriggered	240	400
GW170809	Untriggered	Untriggered	110	190
GW170814	Untriggered	Untriggered	120	200
GW170817	Untriggered	Untriggered	110	190
GW170818	Untriggered	Untriggered	180	330
GW170823	Untriggered	Untriggered	260	500
GW190408_181802	No data	No data	—	—
GW190412	Untriggered	Untriggered	170	280
GW190421_213856	Untriggered	Untriggered	210	400
GW190425	Untriggered	Untriggered	120	190
GW190426_152155	44.7 s	Untriggered	13	19
GW190503_185404	Untriggered	Untriggered	150	270
S190510g	Untriggered	Untriggered	170	280
GW190512_180714	Untriggered	Untriggered	190	330
GW190513_205428	24.7 s	Untriggered	14	20
GW190517_055101	Untriggered	Untriggered	120	200
GW190519_153544	Untriggered	Untriggered	140	250
GW190521	45.0 s	45.0 s	6	10
GW190521_074359	Untriggered	Untriggered	170	280
GW190602_175927	45.0 s	45.0 s	6	12
GW190630_185205	45.0 s	45.0 s	5	9
GW190701_203306	45.0 s	45.0 s	6	11
GW190706_222641	45.0 s	17.5 s	2.5	5
GW190707_093326	Untriggered	Untriggered	220	400
GW190413_052954	Untriggered	Untriggered	170	280
GW190413_134308	Untriggered	Untriggered	160	270
GW190424_180646	Untriggered	Untriggered	140	240
GW190514_065416	Untriggered	Untriggered	280	500
GW190527_092055	Untriggered	Untriggered	140	240
GW190620_030421	Untriggered	Untriggered	270	400
GW190708_232457	Untriggered	Untriggered	150	270
S190718y	18.3 s	Untriggered	17	23
GW190719_215514	Untriggered	Bad	—	—
GW190720_000836	45.0 s	45.0 s	4	6
GW190727_060333	45.0 s	45.0 s	5	9
GW190728_064510	45.0 s	29.6 s	3.2	5
GW190731_140936	Untriggered	Untriggered	210	400
GW190803_022701	Untriggered	Untriggered	140	230
GW190814	45.0 s	Untriggered	14	22
GW190828_063405	45.0 s	18.1 s	6	10
GW190828_065509	45.0 s	Untriggered	16	21
S190901ap	45.0 s	45.0 s	3.1	6
GW190909_114149	Untriggered	Untriggered	110	190
S190910d	45.0 s	45.0 s	4	7
S190910h	45.0 s	45.0 s	2.7	5
GW190910_112807	Untriggered	Untriggered	120	190
GW190915_235702	45.0 s	45.0 s	3.0	6
S190923y	45.0 s	45.0 s	3.2	6
GW190924_021846	45.0 s	45.0 s	4	7
GW190929_012149	Untriggered	Untriggered	200	340
GW190930_133541	45.0 s	45.0 s	7	13
S190930t	45.0 s	45.0 s	5	10
S191105e	Untriggered	Untriggered	180	310
S191109d	45.0 s	45.0 s	5	8
S191129u	Untriggered	Untriggered	230	400
S191204r	Untriggered	Untriggered	300	500
S191205ah	45.0 s	45.0 s	2.7	6
S191213g	45.0 s	45.0 s	3.4	7
S191215w	45.0 s	45.0 s	4	7
S191216ap	45.0 s	29.5 s	2.7	5
S191222n	45.0 s	45.0 s	4	7
S200105ae	Untriggered	Untriggered	230	400
S200112r	45.0 s	No data	16	23
S200114f	45.0 s	45.0 s	9	15
S200115j	45.0 s	45.0 s	2.1	4
S200128d	45.0 s	45.0 s	5	8
S200129m	45.0 s	45.0 s	3.2	6
S200208q	45.0 s	45.0 s	5	7
S200213t	45.0 s	45.0 s	5	10
S200219ac	Untriggered	Untriggered	190	300
S200224ca	45.0 s	No data	22	29
S200225q	45.0 s	45.0 s	3.4	6
S200302c	45.0 s	45.0 s	4	8
S200311bg	45.0 s	No data	16	21
S200316bj	45.0 s	45.0 s	2.9	5

Now a cluster may have 2 to 7 hits associated in time and space. Clusters of greater than 7 hits are rejected as being too large to have been produced by a supernova neutrino interaction. In the ND, we allow clusters with all hits in a single view. However, at the FD, 3-dimensional position information is essential for reducing background, so clusters must include hits in both views. Similarly, ND clusters may be non-contiguous, with gaps either between hits within a detector plane or between detector planes, but FD clusters must be contiguous to reduce background. Previously, we excluded the muon catcher region of the ND; clusters in this region are now accepted.

Critical to the reduction of background, particularly at the FD, is the inclusion of several new variables in the classifier that relate the distance in time and space between candidate hit clusters and recent cosmic rays. Michel electrons from stopping muons are a common background in the FD, occurring at a rate of 40 kHz. Most Michel electrons are identified by close association with track ends, but a small fraction of apparent Michel electrons appear far from the track end, either because of reconstruction failures, inefficiencies in producing hits, complex particle interactions, or some combination of these. Candidate clusters are judged based on their proximity to the track end, to any point along the track, as well as to any hit in a large cluster of activity with no reconstructed tracks.

Supernova neutrino-like hit clusters are separated into signal and background samples using the scikit-learn [44] package's `RandomForestClassifier` class. The classifier is trained with simulated 9.6 $M_\odot$ supernova interactions and real minimum-bias data from the NOvA detectors. The classifier was optimized separately for the ND and the FD. Further, it is optimized separately for the two cases of FD data — continuous readout and pulser. The pulser data must be treated differently because the look-back time for cosmic rays that may have produced a background cluster is reduced. Additionally, since the livetime is smaller, efficiency is prioritized over background reduction. In all three cases, the figure of merit [45]

$$\frac{\text{signal}}{a/2 + \sqrt{\text{background}}},$$

is optimized, with $a = 1.292$ to optimize 90% C.L. limits. The resulting efficiencies for IBD positrons are shown in Fig. 1. Efficiencies for ES electrons, as a function of electron energy, are very similar. At the ND, neutron captures from IBD are selected with 2% efficiency, while at the FD the neutron capture efficiency is negligible for purposes of the signal: only 0.02%. No attempt is made in the analysis to associate positron and neutron delayed coincidences in either detector.

Compared with our previous analysis method, the rate of selected background candidates in the FD, for continuous readout, is reduced by a factor of eighty, from 460 Hz to 6 Hz, while the signal efficiency is reduced from 7.8% to 4.3%. In the previous analysis, the same selection was used for FD continuous-readout and FD pulser data. In this analysis, the pulser background rate is reduced to 55 Hz, while the signal efficiency is increased to 9.0%, or 0.3 Hz and 0.05% taking into account the 0.55% livetime. In the ND, the rate of selected background candidates has been slightly reduced from 0.5 Hz to 0.4 Hz while the signal efficiency has been increased from 12% to 44%.

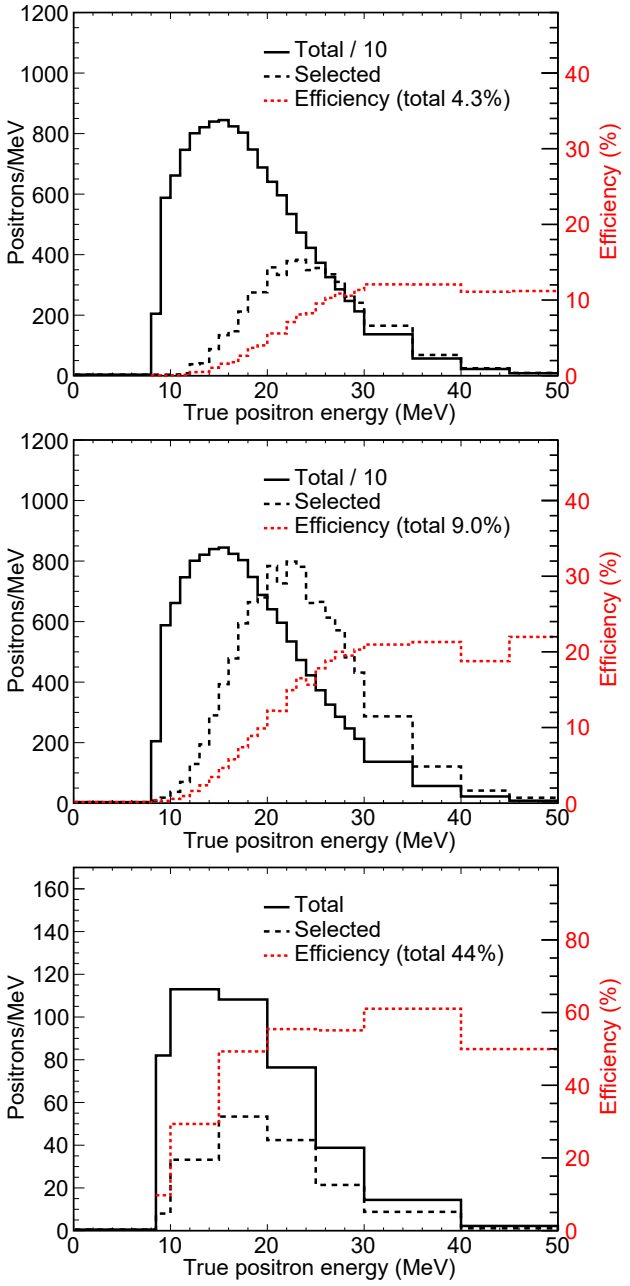

FIG. 1. Top (middle, bottom): FD continuous readout (FD pulser, ND) total and selected positron spectra (left axis) and positron selection efficiency (right axis) as a function of energy. Each plot shows a simulated 9.6 $M_\odot$ supernova at 1 kpc. The total efficiencies, integrated over neutrino energy, are shown in the legends and assume a 9.6 $M_\odot$ supernova; total efficiencies are higher for the 27 $M_\odot$ model.

Since the neutrino event classifier is trained on real detector data, no explicit identification of the background components is made. The FD background likely contains significant components from cosmogenic thermal neutron captures, cosmogenic ^{12}B and ^{12}N beta decays, and single-hit uranium/thorium-chain radioactivity paired with unrelated single-hit electronics noise. The latter is possibly a significant component of the ND background as well, but cosmogenic activity is strongly suppressed compared to the FD.

For 16 of the 40 GW events with ND data, the NuMI beam was in operation. Data at the ND is taken in 5 ms segments. Any 5 ms data segment is rejected if it overlaps with a beam pulse or the time up to 3 ms following a beam pulse. This conservative cut removes all prompt beam activity, muon decays, and neutron captures from thermal neutrons that were produced in the detector and remained in the detector until captured. Some neutron captures can be delayed up to several milliseconds if thermal neutrons spend time in the air surrounding the detector; the 3 ms cut rejects a large majority of these neutrons.

For each gravitational wave event, we first examine the selected clusters in 1-second bins searching for any significant excess over background, where the background level is determined *in situ* from the 45 s readout (or 1000 s window in the case of FD pulser data). Second, we assume that a supernova burst begins at the gravitational wave timestamp and set limits on its strength for the case of the Garching 9.6 $M_\odot$ and 27 $M_\odot$ models. Because NOvA's efficiency rises rapidly with neutrino energy between 10 and 30 MeV, the higher neutrino energies in the 27 $M_\odot$ model result in stronger fluence limits.

Depending on the state of the two NOvA detectors and whether a trigger was received from LVC, several different types of data sets can be available. The best case is when a timely trigger was received and we read 45 s of continuous data from the ND and FD. In this case, a joint analysis is done using the data from the two detectors. The FD provides more statistical power, but the ND still makes a significant contribution. In some cases, continuous data is available from the ND, but only pulser data from the FD. Again, a joint analysis is performed, but in this case, the ND provides nearly all the statistical power. In some cases, the continuous data from ND or FD is not a complete 45 s, but in all those cases enough was read out to establish the background level and allow the analysis to be run without modification. The background level is not determined with as much precision in these cases, leading to a slight weakening of limits. Finally, in some cases, data from only one detector is available. The status for all GW events is shown in Table I.

VI. RESULTS

No excess over background is observed for any gravitational wave event at any time within the analyzed window. Background rates were stable at both detectors,

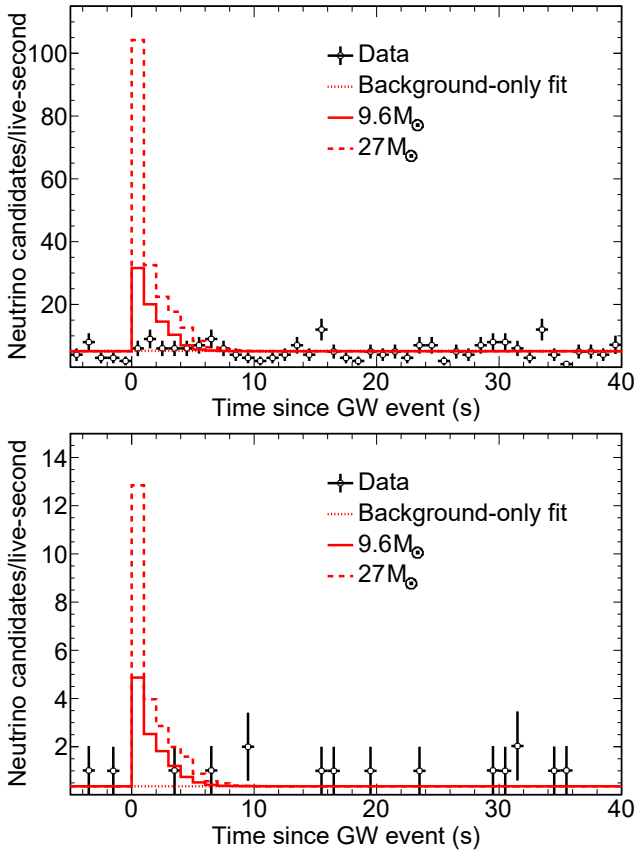

FIG. 2. A typical GW event with both FD (top) and ND (bottom) continuous readout, S200213t. The two supernova models are shown, normalized to 10 kpc. The number of neutrino candidates per second is corrected for livetime, which is slightly under 100% in the ND because of beam removal, and in the final bins because readout ends at 39.86 s. The limits set are weaker than the median case because of a slight excess in the 0–5 s bins in the statistically-dominant FD.

being around 5 Hz at the FD for the continuous-readout selection, 0.3 Hz for the FD pulser selection and 0.4 Hz at the ND. Assuming all selected clusters are background, the limits depend on statistical fluctuations in the background in the first few seconds after the gravitational wave timestamp. A typical event is shown in Fig. 2.

For each GW event, 90% C.L. limits are set on the fluence of the sum of all neutrino flavors, F, under the assumption of the two Garching supernova models discussed above, without flavor-changing effects. The limits are set via a fit to the time series of neutrino candidates with two parameters: the background rate and the signal strength, with the signal templates as shown in Fig. 2. A Bayesian approach is used with flat priors in each parameter.

A posterior PDF, profiled over the background level, is constructed by scanning over signal strength, relative to the prediction at 10 kpc, in steps of 10^{-3}. At each step,

the binned log-likelihood,

$$-\log L = \sum_{\mathrm{i}} \left(m_i - d_i + d_i \log \frac{d_i}{m_i} \right)$$

is computed for the background normalization that minimizes $-\log L$, where m_i is the number of events predicted by the model in bin i and d_i is the number of events observed, likewise. The probability density is proportional to L. The resulting curve is integrated numerically up to 90% of the total, and this sets the 90% upper limit on signal strength, s_{90}. Because the signal would decrease as $1/r^2$, where r is the distance to the hypothetical supernova, the 90% lower limit on distance is $r_{90} = 10\,\mathrm{kpc}/\sqrt{s_{90}}$. Given the number of neutrinos predicted by each model, $N = 6.8(11) \times 10^{57}$ for $9.6(27)\,\mathrm{M}_\odot$, fluence limits, F_{90}, are related to the distance limits via

$$F_{90} = \frac{N}{4\pi r_{90}^2}.$$

No systematic effects are explicitly included in the procedure, but as detailed in Section IV, our estimate of the rate of detectable neutrino interactions is conservative; we believe this conservatism is sufficient to cover any systematic effects in signal efficiency. All limits are shown in Table I and a discussion of notable features thereof follows.

For gravitational wave events in which we read out continuous FD data in response to an LVC trigger (the best case), fluence limits range between $F < 4 \times 10^{10}\,\mathrm{cm}^{-2}$ and $F < 15 \times 10^{10}\,\mathrm{cm}^{-2}$, assuming the $9.6\,\mathrm{M}_\odot$ Garching model. In this model, 22% of the neutrinos are $\bar{\nu}_\mathrm{e}$, to which NOvA is primarily sensitive. The median limit is $7 \times 10^{10}\,\mathrm{cm}^{-2}$. Similarly, for the $27\,\mathrm{M}_\odot$ model, in which 23% of the flux is $\bar{\nu}_\mathrm{e}$, we set limits ranging from $F < 2.1 \times 10^{10}\,\mathrm{cm}^{-2}$ to $F < 9 \times 10^{10}\,\mathrm{cm}^{-2}$ with a median of $4 \times 10^{10}\,\mathrm{cm}^{-2}$. If interpreted as limits on the distance to a hypothetical supernova, we exclude a $9.6\,\mathrm{M}_\odot$ supernova in the median case, at 90% C.L., closer than 29 kpc. For the event with the strongest exclusion, S200115j, we exclude a $9.6\,\mathrm{M}_\odot$ supernova closer than 40 kpc. For the $27\,\mathrm{M}_\odot$ model, we exclude a supernova, in the median case, closer than 50 kpc, and for S200115j, 70 kpc.

In the next best case, we have continuous ND data, but either have no FD data or only pulser data from the FD data. In the latter case, the limit is strongly dominated by the ND data. Fluence limits for the $9.6\,\mathrm{M}_\odot$ model range from $F < 19 \times 10^{10}\,\mathrm{cm}^{-2}$ to $F < 29 \times 10^{10}\,\mathrm{cm}^{-2}$, and for the $27\,\mathrm{M}_\odot$ from $F < 13 \times 10^{10}\,\mathrm{cm}^{-2}$ to $F < 22 \times 10^{10}\,\mathrm{cm}^{-2}$. Because of the ND's lower background, the efficiency for selecting lower energy neutrinos is higher than the FD. The flux model therefore has less effect on fluence limits dominated by ND data. The median distance limit for a $9.6(27)\,\mathrm{M}_\odot$ supernova is 16(24) kpc.

Finally, when using only FD pulser data, fluence limits range from $F < 190 \times 10^{10}\,\mathrm{cm}^{-2}$ to $F < 700 \times 10^{10}\,\mathrm{cm}^{-2}$ for the $9.6\,\mathrm{M}_\odot$ model and from $F < 110 \times 10^{10}\,\mathrm{cm}^{-2}$ to $F < 400 \times 10^{10}\,\mathrm{cm}^{-2}$ for the $27\,\mathrm{M}_\odot$ model. Even with only FD pulser data, some exclusion of supernovae in or behind the Galactic core (at ~ 8 kpc), whose optical signal may have been obscured, is possible, with distance limits ranging from 2.9–6 kpc for the $9.6\,\mathrm{M}_\odot$ case and 5–9 kpc for the $27\,\mathrm{M}_\odot$ case.

The 26 GW events analyzed in our previous report are reanalyzed using the improved analysis. The limits quoted for the seven previously-analyzed events that include FD and/or ND continuous readout are now stronger, in the median case, by a factor of three, and in no case is the result we now give weaker than our previously published result. However, for events with only FD pulser data, the new analysis techniques only yield a 40% improvement in fluence limits. There are four GW events that, in the new analysis, have a weaker limit for at least one of the two supernova models, GW170608, GW170729, GW170823 and GW190521_074359. This is an expected consequence of using an analysis that is almost entirely different than our previous analysis, such that there is little correlation between the hits selected previously and now.

VII. CONCLUSIONS

We have searched for supernova-like neutrinos coincident with 76 gravitational wave events reported by LVC. No excess consistent with such neutrinos is found. Assuming a burst of supernova-like neutrinos beginning at LVC's reconstructed gravitational wave time, we set limits on the fluence of supernova-like neutrinos under two supernova models. In the 32 cases with full FD data, these limits are sufficient to largely exclude the possibility that any of the gravitational waves originated from a stellar core collapse in our galaxy. This includes the "failed supernovae" in which there is no explosion and/or scenarios that lead to early black hole formation, since similar neutrino luminosities are expected in any of these cases [46, 47]. Our search complements those performed by other neutrino observatories [48–55]. The NOvA detectors will continue to operate for several years, including during the upcoming O4 run of LVC.

This document was prepared by the NOvA collaboration using the resources of the Fermi National Accelerator Laboratory (Fermilab), a U.S. Department of Energy, Office of Science, HEP User Facility. Fermilab is managed by Fermi Research Alliance, LLC (FRA), acting under Contract No. DE-AC02-07CH11359. This work was supported by the U.S. Department of Energy; the U.S. National Science Foundation; the Department of Science and Technology, India; the European Research Council; the MSMT CR, GA UK, Czech Republic; the RAS, RFBR, RMES, RSF, and BASIS Foundation, Russia; CNPq and FAPEG, Brazil; STFC, UKRI, and the Royal Society, United Kingdom; and the State and University of Minnesota. We are grateful for the contributions of the staffs of the University of Minnesota at the Ash River Laboratory and of Fermilab.

[1] B. P. Abbott *et al.* (LIGO Scientific Collaboration and Virgo Collaboration), GW170817: Observation of gravitational waves from a binary neutron star inspiral, Phys. Rev. Lett. **119**, 161101 (2017), arXiv:1710.05832.

[2] A. Goldstein *et al.*, An ordinary short gamma-ray burst with extraordinary implications: Fermi-GBM detection of GRB 170817A, Astrophys. J. **848**, L14 (2017), arXiv:1710.05446.

[3] B. P. Abbott *et al.* (LIGO Scientific, Virgo, Fermi-GBM, INTEGRAL), Gravitational waves and gamma-rays from a binary neutron star merger: GW170817 and GRB 170817A, Astrophys. J. **848**, L13 (2017), arXiv:1710.05834.

[4] R. Abbott *et al.* (LIGO Scientific Collaboration, Virgo Collaboration), GWTC-2: Compact binary coalescences observed by LIGO and Virgo during the first half of the third observing run, 2010.14527 (2020).

[5] B. P. Abbott *et al.* (LIGO Scientific Collaboration, Virgo Collaboration), A first targeted search for gravitational-wave bursts from core-collapse supernovae in data of first-generation laser interferometer detectors, Phys. Rev. **D94**, 102001 (2016), arXiv:1605.01785.

[6] S. M. Adams, C. S. Kochanek, J. F. Beacom, M. R. Vagins, and K. Z. Stanek, Observing the next galactic supernova, Astrophys. J. **778**, 164 (2013), arXiv:1306.0559.

[7] M. A. Acero *et al.* (NOvA), Search for multimessenger signals in NOvA coincident with LIGO/Virgo detections, Phys. Rev. D **101**, 112006 (2020), arXiv:2001.07240.

[8] D. S. Ayres *et al.* (NOvA), The NOvA technical design report, FERMILAB-DESIGN-2007-01 (2007).

[9] P. Adamson *et al.*, The NuMI Neutrino Beam, Nucl. Instrum. Meth. **A806**, 279 (2016), arXiv:1507.06690.

[10] B. P. Abbott *et al.* (LIGO Scientific Collaboration, Virgo Collaboration), GWTC-1: A gravitational-wave transient catalog of compact binary mergers observed by LIGO and Virgo during the first and second observing runs, Phys. Rev. **X9**, 031040 (2019), arXiv:1811.12907.

[11] LIGO Scientific Collaboration and Virgo Collaboration, S190510g, GCN Circular 24442 (2019).

[12] LIGO Scientific Collaboration and Virgo Collaboration, S190718y, GCN 25087 (2019).

[13] LIGO Scientific Collaboration and Virgo Collaboration, S190901ap, GCN 25606 (2019).

[14] LIGO Scientific Collaboration and Virgo Collaboration, S190910d, GCN 25695 (2019).

[15] LIGO Scientific Collaboration and Virgo Collaboration, S190910h, GCN 25707 (2019).

[16] LIGO Scientific Collaboration and Virgo Collaboration, S190923y, GCN 25814 (2019).

[17] LIGO Scientific Collaboration and Virgo Collaboration, S190930t, GCN 25876 (2019).

[18] LIGO Scientific Collaboration and Virgo Collaboration, S191105e, GCN 26182 (2019).

[19] LIGO Scientific Collaboration and Virgo Collaboration, S191109d, GCN 26202 (2019).

[20] LIGO Scientific Collaboration and Virgo Collaboration, S191129u, GCN 26303 (2019).

[21] LIGO Scientific Collaboration and Virgo Collaboration, S191204r, GCN 26334 (2019).

[22] LIGO Scientific Collaboration and Virgo Collaboration, S191205ah, GCN 26350 (2019).

[23] LIGO Scientific Collaboration and Virgo Collaboration, S191213g, GCN 26402 (2019).

[24] LIGO Scientific Collaboration and Virgo Collaboration, S191215w, GCN 26441 (2019).

[25] LIGO Scientific Collaboration and Virgo Collaboration, S191216ap, GCN 26454 (2019).

[26] LIGO Scientific Collaboration and Virgo Collaboration, S191222n, GCN 26543 (2019).

[27] LIGO Scientific Collaboration and Virgo Collaboration, S200105ae, GCN 26640 (2020).

[28] LIGO Scientific Collaboration and Virgo Collaboration, S200112r, GCN 26715 (2020).

[29] LIGO Scientific Collaboration and Virgo Collaboration, S200114f, GCN 26734 (2020).

[30] LIGO Scientific Collaboration and Virgo Collaboration, S200115j, GCN 26759 (2020).

[31] LIGO Scientific Collaboration and Virgo Collaboration, S200128d, GCN 26906 (2020).

[32] LIGO Scientific Collaboration and Virgo Collaboration, S200129m, GCN 26926 (2020).

[33] LIGO Scientific Collaboration and Virgo Collaboration, S200208q, GCN 27014 (2020).

[34] LIGO Scientific Collaboration and Virgo Collaboration, S200213t, GCN 27042 (2020).

[35] LIGO Scientific Collaboration and Virgo Collaboration, S200219ac, GCN 27130 (2020).

[36] LIGO Scientific Collaboration and Virgo Collaboration, S200224ca, GCN 27184 (2020).

[37] LIGO Scientific Collaboration and Virgo Collaboration, S200225q, GCN 27193 (2020).

[38] LIGO Scientific Collaboration and Virgo Collaboration, S200302c, GCN 27278 (2020).

[39] LIGO Scientific Collaboration and Virgo Collaboration, S200311bg, GCN 27358 (2020).

[40] LIGO Scientific Collaboration and Virgo Collaboration, S200316bj, GCN 27388 (2020).

[41] A. Mirizzi, I. Tamborra, H. Janka, N. Saviano, K. Scholberg, R. Bollig, L. Hudepohl, and S. Chakraborty, Supernova neutrinos: Production, oscillations and detection, Riv. Nuovo Cim. **39**, 1 (2016), arXiv:1508.00785.

[42] C. Andreopoulos *et al.*, The GENIE neutrino Monte Carlo generator, Nucl. Instrum. Meth. **A614**, 87 (2010), arXiv:0905.2517.

[43] S. Agostinelli *et al.*, Geant4 - a simulation toolkit, Nucl. Instrum. Meth. **A506**, 250 (2003).

[44] F. Pedregosa *et al.*, Scikit-learn: Machine learning in Python, Journal of Machine Learning Research **12**, 2825 (2011).

[45] G. Punzi, Sensitivity of searches for new signals and its optimization (2003), arXiv:physics/0308063.

[46] A. da Silva Schneider, E. O'Connor, E. Granqvist, A. Betranhandy, and S. M. Couch, Equation of state and progenitor dependence of stellar-mass black hole formation, Astrophys. J. **894**, 4 (2020).

[47] S. W. Li, L. F. Roberts, and J. F. Beacom, Exciting prospects for detecting late-time neutrinos from core-collapse supernovae, Phys. Rev. D **103**, 023016 (2021).

[48] M. Agostini *et al.*, A search for low-energy neutrinos correlated with gravitational wave events GW150914, GW151226 and GW170104 with the Borexino detector, Astrophys. J. **850**, 21 (2017), arXiv:1706.10176.

[49] A. Gando *et al.* (KamLAND), Search for electron antineutrinos associated with gravitational wave events GW150914 and GW151226 using KamLAND, Astrophys. J. **829**, L34 (2016), arXiv:1606.07155.

[50] S. Abe *et al.* (KamLAND), Search for low-energy electron antineutrinos in KamLAND associated with gravitational wave events, Astrophys. J. **909**, 116 (2021), arXiv:2012.12053 [astro-ph.HE].

[51] K. Abe *et al.* (Super-Kamiokande), Search for neutrinos in Super-Kamiokande associated with gravitational wave events GW150914 and GW151226, Astrophys. J. **830**, L11 (2016), arXiv:1608.08745.

[52] K. Abe *et al.* (Super-Kamiokande), Search for neutrinos in coincidence with gravitational wave events from the LIGO-Virgo O3a observing run with the Super-Kamiokande detector (2021), arXiv:2104.09196 [astro-ph.HE].

[53] S. Adrian-Martinez *et al.* (Virgo, IceCube, ANTARES, LIGO Scientific), High-energy neutrino follow-up search of gravitational wave event GW150914 with ANTARES and IceCube, Phys. Rev. **D93**, 122010 (2016), arXiv:1602.05411.

[54] A. Albert *et al.* (Virgo, IceCube, ANTARES, LIGO Scientific), Search for high-energy neutrinos from gravitational wave event GW151226 and candidate LVT151012 with ANTARES and IceCube, Phys. Rev. **D96**, 022005 (2017), arXiv:1703.06298.

[55] A. Aab *et al.* (Pierre Auger), Ultrahigh-energy neutrino follow-up of gravitational wave events GW150914 and GW151226 with the Pierre Auger Observatory, Phys. Rev. **D94**, 122007 (2016), arXiv:1608.07378.